THE JOURNAL OF PHYSICAL CHEMISTRY C

pubs.acs.org/JPCC Article

Promoting Z-to-E Thermal Isomerization of Azobenzene Derivatives by Noncovalent Interaction with Phosphorene: Theoretical Prediction and Experimental Study

Dong Zheng, Mengning Ding, Yi Hu, Jun Zhao, Chunyan Liu, Xiang Li, Pingying Liu, Zhong Jin, and Jing Ma*

Cite This: J. Phys. Chem. C 2020, 124, 15961−15968 Read Online

ACCESS | Metrics & More | Article Recommendations | Supporting Information

ABSTRACT: The ability to modulate the rate of Z/E isomerization of azobenzene (AB) derivatives is crucial to the practical applications of biological and photofunctional systems. Four kinds of AB−OC_4H_8−R derivatives (AB-1, R = $NMe_3^+I^-$; AB-2, R = NH_2; AB-3, R = C_6H_{13}; AB-4, R = SH) were incorporated into liquid-exfoliated black phosphorus (BP) nanosheets through noncovalent functionalization. Experiments indicated that the switching process between the two states, *trans* (E) and *cis* (Z), especially the Z-to-E thermal conversion of AB derivatives, was accelerated 2−23 times by the presence of phosphorene at temperatures of 293−313 K. The acceleration phenomenon was rationalized by density functional theory (DFT) calculations, which reveals that the interaction between phosphorene and AB derivatives stabilized the Z isomer and transition state of azobenzene in a less degree than the E isomer, hence lowering the activation energy (E_a) of the Z-to-E isomerization. A close correlation is shown between the extent of charge transfer, the binding energy, and the Z-to-E thermal activation energy. The reactive molecular dynamics simulations also demonstrated a threefold faster isomerization process for AB@BP hybrids to accomplish the thermal relaxation relative to the free-standing AB. The predicted energy difference between E and Z isomers of AB@BP hybrids are enhanced 2−3 times upon deposition on the BP substrate. The photoresponsive AB@BP system suggests a new platform for energy conversion and potential applications in the biological field.

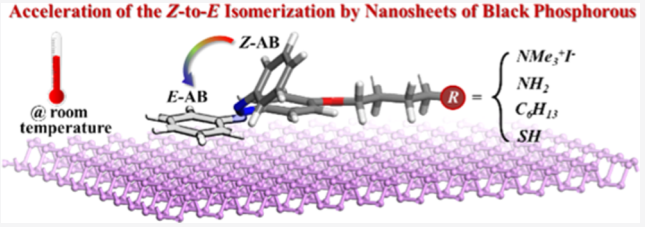

1. INTRODUCTION

Explosive developments have provided new opportunities for biomedical applications using two-dimensional (2D) nanomaterials,[1] which also have numerous potential applications in electronics, optoelectronics, and energy conversion and storage devices.[2−4] Few-layer black phosphorus (BP) is a new member of 2D nanomaterials, which has attracted significant research interest because of its excellent broad UV−vis-to-near-infrared light absorption.[5] The few-layer puckered structure of BP provides ultralarge surface areas for various adsorbed molecules for different purposes such as anticancer treatment and drug delivery.[6]

It is highly desirable that the properties of few-layer 2D materials could be altered on demand in different environments. In other words, the system could respond to external stimuli, such as temperature, light, or acidity of the environment. Among diverse stimuli, light is a fascinating one because it is noninvasive, sustainable, and allows high spatiotemporal precision controlling.[7] The simplest way to introduce a photoresponsive property is to functionalize with a light-responsive unit. There are two methods to hybridize the photoresponsive units into the substrates. One way is to introduce responsive units via covalent chemistry using a multistep synthetic approach. Alternatively, the functionalized assembly can be fabricated by intermolecular noncovalent interactions, which is simple and fast.

Among all types of photoresponsive molecules, azobenzene (AB) has been regarded as a powerful molecular switch and has been applied to a broad range of applications such as liquid crystals and drug delivery vehicles.[8] Taking advantage of the facile E/Z isomerization of the N═N double bonds, the azobenzene derivatives could function as smart switches, which reversibly change between the global minimum of the *trans* (E) isomer and the metastable *cis* (Z) one through the −N═N− rotation (ϕ) or C−N═N inversion (θ) pathways.[9] The geometrical isomerization of the AB derivative is indeed accompanied by an energy conversion: upon the light-driven E-to-Z isomerization, the energy is stored in the Z isomer with the stored energy estimated by the relative energy ΔE_{Z-E} between the Z (E_Z) and E (E_E) isomers, which is further

Received: April 29, 2020
Revised: June 23, 2020
Published: June 26, 2020

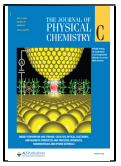

https://dx.doi.org/10.1021/acs.jpcc.0c03837
J. Phys. Chem. C 2020, 124, 15961−15968

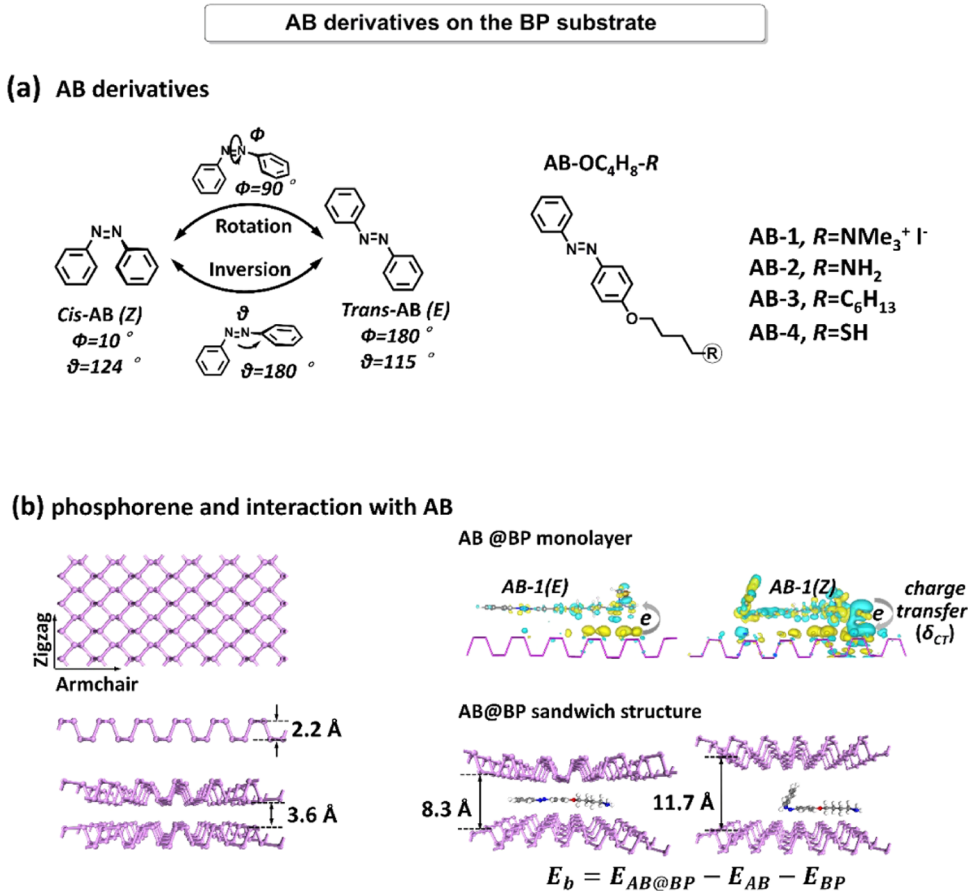

Figure 1. Schematic illustrations of (a) substituted AB derivatives (AB-1, AB-2, AB-3, AB-4) in Z and E forms and the energy difference, ΔE_{Z-E}, between two isomers and (b) phosphorene and its noncovalent interaction with AB derivatives, evaluated by the binding energy, E_b.

released during the inverse Z-to-E transition. The incorporation of AB derivatives into some nonmetal low-dimensional materials (e.g., graphene and arsenene) has been demonstrated experimentally or theoretically to bring new opportunities to form novel hybrid materials.[10−14] The AB derivatives were also incorporated into DNA-based motifs to trigger the reversible and cyclic configuration of constitutional dynamic networks.[15] However, the detailed understanding of the unique interaction between photoresponsive molecules and phosphorene under the external triggers remains to be explored. It is also of importance to realize the Z/E isomerization of azobenzene derivatives at room temperature, allowing future applications in bioactive systems.

In the present work, the conformationally flexible alkoxy-modified azobenzene derivatives were selected to combine with the layered phosphorene. More specifically, only one end of the aromatic benzene ring is substituted by an alkoxy group with different terminal groups, which are electron-donating or -withdrawing groups. The benzene ring with a substituted long alkoxy chain could interact with the phosphorene, while the unsubstituted benzene could either lying or tilting upon the phosphorene surface. Hence, we fabricated four kinds of AB@BP systems containing AB−OC_4H_8−R derivatives: 1-butanaminium,*N*,*N*,*N*-trimethyl-4-(4-(2-phenyldiazenyl)phenoxy)-, iodine (1:1) (AB-1, R = $NMe_3^+I^-$); 4-(4-(2-phenyldiazenyl)-phenoxy)-1-butanamine (AB-2, R = NH_2) with a proton-accepting amino group; 1-(4-(decyloxy)-2-phenyldiazene) (AB-3, R = C_6H_{13}) with a hydrophobic chain; and 4-(4-(2-phenyldiazenyl)phenoxy)-1-butanethiol (AB-4, R = SH) with a proton-donating thiol group (Figure 1a). Among them, the trimethylammonium iodine-substituted azobenzene (AB-1) shows the highest acceleration (23 times) of the Z-to-E isomerization rate constant by deposition on the phosphorene surface at 293 K. Density functional theory (DFT) calculations revealed that the strongest interfacial charge transfer occurred between a polar trimethylammonium iodine group (R = $NMe_3^+I^-$) and a BP substrate (Figure 1b). The strong interaction between BP and AB, which is evaluated by the binding energy (E_b), stabilizes the Z isomer and the transition-state structure in a less degree than the E isomer and therefore lowers the activation energy (E_a) of the Z-to-E isomerization. We also found that noncovalent functionalization with AB derivatives led to considerable stabilization of the freshly exfoliated BP. The easily adjustable thermal Z-to-E isomerization through noncovalent functionalization on phosphorene shows potential applications in energy conversion and biomedical usage.

2. METHODS

2.1. Experimental Section. The isomerization process was studied by UV−vis absorption spectra, which were obtained from UV-2600 (Shimadzu, Japan) using a quartz glass cell with a path length of 10 mm at different temperatures. The rate constants (k) of the Z-to-E isomerization in the dark at different temperatures were determined from the equation derived on the assumption of the first-order kinetics of the isomerization reaction and the applicability of the Lambert−Beer law

https://dx.doi.org/10.1021/acs.jpcc.0c03837
J. Phys. Chem. C 2020, 124, 15961−15968

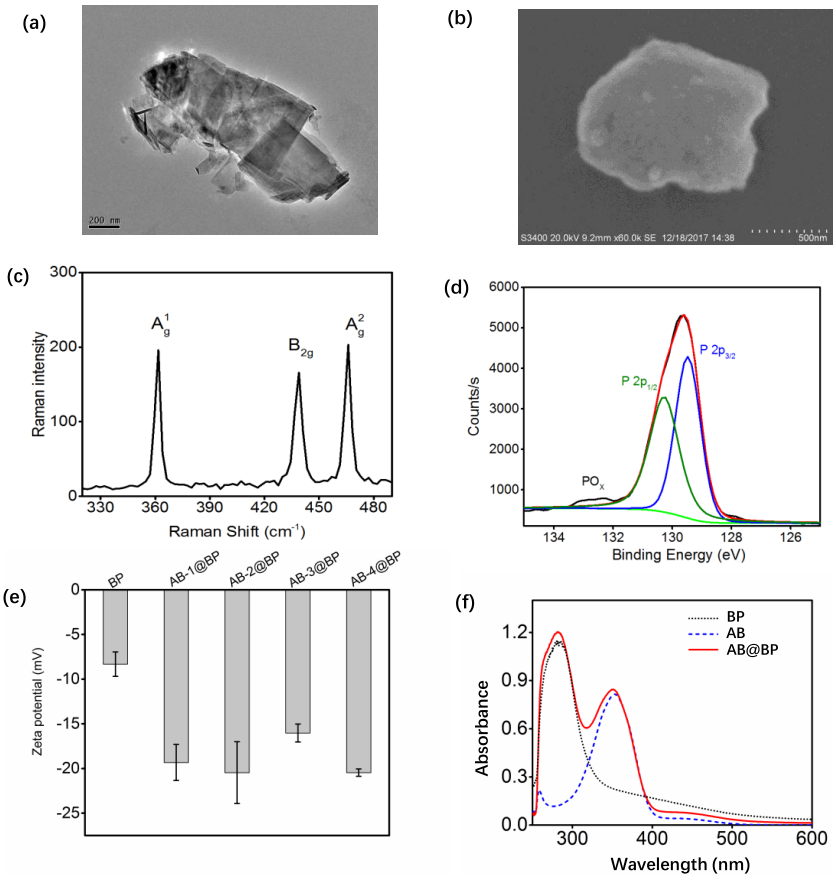

Figure 2. Characterization of BP nanomaterials. (a) TEM and (b) SEM images of BP nanosheets; (c) Raman spectra of BP nanosheets; (d) XPS spectra of BP nanosheets; (e) ζ-potential of the BP nanomaterials and the AB@BP complexes; and (f) UV−vis spectra of AB, BP, and AB@BP in the DMSO solution.

$$\ln\left(\frac{A_0 - A_\infty}{A_t - A_\infty}\right) = kt \tag{1}$$

where A_0 corresponds to the initial absorbance, A_t is the momentary absorbance, and the A_∞ is the absorbance in the equilibrium. The values of A_0, A_t, and A_∞ were measured at a wavelength of 352 nm. The temperature dependences of the rate constants of thermal Z-to-E isomerization were expected to follow the Arrhenius equation

$$\ln k = -\frac{E_a}{RT} + \ln A \tag{2}$$

where E_a is the activation energy of the reaction, A is the pre-exponential factor, R is the gas constant, and T is the temperature in the absolute scale. The evaluated E_a values were obtained from Arrhenius plots.

2.2. Computational Details. For the isolated (AB-1, R = $NMe_3^+I^-$; AB-2, R = NH_2; AB-3, R = C_6H_{13}; AB-4, R = SH) molecules, DFT calculations with the B3LYP functional and the 6-311+G(d,p) basis set were performed with the Gaussian 09 package suite.[16] Frequency calculations at the same level of theory were carried out to characterize each stationary point (minimum or transition state). Time-dependent density functional theory (TD-DFT) was used to calculate the low-lying excitation energies of the dipole-allowed transitions for AB derivatives at the CAM-B3LYP/6-311+G(d,p) level.

As for the AB@BP hybrids, the DFT computations were performed using the projector augmented planewave (PAW) scheme as implemented in the Vienna ab initio simulation package (VASP)[17,18] using the slab model and periodic boundary condition (PBC). We make use of the generalized approximation (GGA) formulated by Perdew, Burke, and Ernzerhof (PBE) as the exchange−correlation functional.[19] A 6 × 4 unit cell of the black phosphorus monolayer (96 phosphorus atoms) and bilayer (192 phosphorus atoms) was chosen as the supercell. The E/Z-AB derivatives were physisorbed onto the monolayer or in a sandwich model, respectively. A 30 Å vacuum layer was used to avoid possible interactions between periodic images. A 3 × 3 × 1 Monkhorst−Pack[20] k-point mesh was used for the Brillouin zone integration in geometry relaxations. The convergence threshold of the geometry optimizations was set to be 10^{-5} eV in energy and 0.01 eV·Å^{-1}. A 500 eV cutoff was used for the planewave basis set. A complete linear synchronous transit (LST)/quadratic synchronous transit (QST)[21] protocol was employed for the TS searching of free-standing AB and AB@BP composites using the Materials Studio CASTEP module[22] with an energy cutoff of 340 eV.

Adsorption energies E_b of adsorbate azobenzene derivatives on phosphorene were calculated by subtracting the DFT-calculated energies of adsorbate AB derivatives (E_{AB}) and clean phosphorene (E_{BP}) from the energy of the composite ($E_{AB@BP}$), as shown in the formula

$$E_b = E_{AB@BP} - E_{AB} - E_{BP} \tag{3}$$

https://dx.doi.org/10.1021/acs.jpcc.0c03837
J. Phys. Chem. C 2020, 124, 15961−15968

To understand the physical nature of the interaction between AB derivatives and phosphorene, the electron density was examined. For a fully optimized geometry, the electron density difference was calculated by subtracting the electron densities of the individual species within the geometry of the complex from the electron density of the whole complex as

$$\Delta\rho = \rho_{AB@BP} - \rho_{AB} - \rho_{BP} \quad (4)$$

where ρ_{AB} and ρ_{BP} represent the electron densities of AB derivatives and phosphorene with the geometry of the complex, respectively. $\rho_{AB@BP}$ represents the electron density of complex AB@BP. The electron density difference maps were generated using the VESTA package.[23]

The reactive molecular dynamics (RMD) simulations,[24−28] which were developed by our group, were successfully applied to trace the dynamic process of isomerization of various azobenzene-containing complex systems in the condensed phase. Modifications on the C−N═N−C torsion potential and C−N═N inversion potential were implemented on the polymer consistent force filed (PCFF[29]) in RMD simulations. The corresponding torsion force function of the N═N bond and the inversion force function of the C−N═N angle in the simulations are given as

$$E_{torsion}(\phi) = K_\phi(1 + \cos(n\phi - \phi_0)) \quad (5)$$

$$E_{bend}(\theta) = K_\theta(\theta - \theta_0)^2 \quad (6)$$

where K_ϕ is set as the lowest vertical excitation energy, which comes from the TD-DFT calculations or experimental UV−vis absorption spectra. We used a canonical NVT ensemble at 298 K with a Nose thermostat and the velocity Verlet algorithm with a time step of 1 fs. All of the systems employ the periodic boundary condition (PBC) model with a time scale of 50 ps. Twenty independent simulations were performed starting from the Z form of AB derivatives.

3. RESULTS AND DISCUSSION

3.1. Characterization of AB@BP Nanosheets. The ^{1}H nuclear magnetic resonance (NMR) spectra of *para*-substituted AB derivatives are shown in Figure S1. BP nanosheets were produced by the liquid-phase exfoliation method through the sonication of bulk BP crystals in dimethyl sulfoxide (DMSO) solvent, and the details are presented in Figures S2 and S3. The transmission electron microscopy (TEM), scanning electron microscopy (SEM), and atomic force microscopy (AFM) images show that the BP nanosheets have an average lateral size of 100−400 nm and a thickness of 10 nm (Figures 2a,b and S4). With the assistance of AB derivatives, the exfoliated BP nanosheets show a reduced thickness and an increased lateral size (Figure S5). As shown in Figure 2c, three Raman peaks with frequencies of 362, 439, and 466 cm^{-1} correspond to A_g^1 (out-of-plane phonon mode), B_{2_g} (in-plane mode), and A_g^2 (in-plane mode) of BP and are consistent with the Raman features of crystalline BP nanosheets.[30] The X-ray photoelectron spectra (XPS) showed that the as-prepared BP flakes have $2p^{3/2}$ and $2p^{1/2}$ doublets at 129.6 and 130.7 eV, respectively, which are characteristic of crystalline BP (Figure 2d).[31]

The ζ-potential of free-standing BP nanosheets was different from that of the AB@BP hybrids (Figure 2e). Also, the UV−vis spectra of AB@BP contain characteristic absorption peaks of BP (283 nm) and AB derivatives (352 nm), which is shown in Figure 2f. Both the ζ-potential and UV−vis spectra revealed the complexation of AB derivatives with BP nanosheets.

3.2. Electronic Structure of AB Derivatives. Upon UV irradiation, azobenzene derivatives (AB-1−AB-4) with different lengths of the alkyl chain and different terminal groups exhibit big changes in molecular size and polarity, which makes it possible to construct smart nanosystems with photoresponsive properties. DFT calculations reveal that the cationic azobenzene surfactant (AB-1, R = $NMe_3^+I^-$) shows much large dipole moment (Z, 13.3 D; E, 10.5 D) than the other AB derivatives (AB-2−AB-4) due to the strong electrostatic interaction between the trimethylammonium ion and anion (Figure S6). This implies the significant interaction of AB derivatives with the BP substrate, which will be demonstrated later in experiments and calculations. The cetyl-trimethylammonium bromide was used as a charged surfactant to produce monolayer phosphorene through an electrochemical molecular intercalation approach.[32] AB derivatives with quaternary ammonium salt substitution are also useful for controlling the opening and closing of the ion channel and the construction of stimuli-responsive host−guest systems.[33−35] The substituted tetra-alkoxy groups with R = NH_2 (AB-2) and R = SH (AB-4) terminal groups are selected to represent two typical substituents with electron-withdrawing and electron-donating properties, respectively. AB derivatives with long alkoxy groups (AB-3, R = C_6H_{13}) are widely employed to enhance the interactions with the incorporated materials.[36] DFT geometrical optimization predicted that the Z-to-E isomerization induced an increase of ca. 5 Å in the end-to-end distance (defined as the length between the two terminal H atoms of the substitution R group and the para-phenyl on the other side), slightly longer than that (4 Å) in unsubstituted AB.

The experimental UV−vis absorption spectra (Figure S7) of AB derivatives (AB-1−AB-4) show nearly identical absorption peaks (E, 352 nm; Z, 442 nm) at 293 K, which were ascribed to the limited change in the geometry of the azobenzene chromophore upon *para* substitution. The absorption peaks at 352 and 442 nm arise from the characteristic $\pi-\pi^*$ and $n-\pi^*$ transitions in the E and Z forms, respectively (Figure S8).

3.3. Kinetics of the Photochromic Z-to-E Isomerization of AB Derivatives with and without Phosphorene. The rate of Z-to-E thermal isomerization is an important factor that determines the usage of AB derivatives. The AZO with a slow thermal isomerization rate can be used in long-term solar thermal storage.[37] Azobenzene with fast Z-to-E conversion can also be used in real-time information transmission.[38] It is also a big challenge to achieve Z/E isomerization of azobenzene derivatives at room temperature. The modulation of Z-to-E isomerization rates from tens to thousands (or even in larger) degrees will pave the way toward the development of light-responsive materials in different kinds of fields and environments. The E, Z isomers of AB derivatives show a distinct difference in UV−vis spectra (Figure 3a). Hence, the slow thermal Z-to-E isomerization can be monitored by UV−vis spectra. We can see in Figure 3b that the hybrid AB@BP system shows much faster Z-to-E conversion compared with the free-standing AB within the same time period (24 h). Acceleration of the thermal conversion was also observed for all AB@BP hybrids (Figures S9−S12). The details of the calculated first-order rate constants (k) and the activation energies (E_a) of the thermal Z-to-E reaction kinetics for AB with and without the BP

https://dx.doi.org/10.1021/acs.jpcc.0c03837
J. Phys. Chem. C 2020, 124, 15961−15968

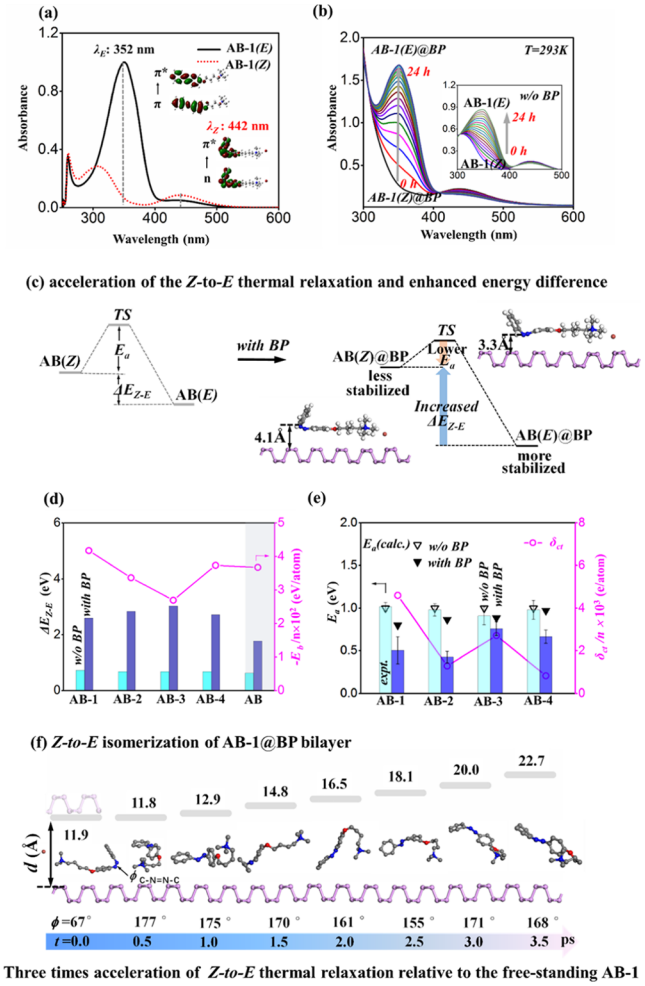

Figure 3. (a) UV−vis absorption spectra of molecule AB-1, R = $NMe_3^+I^-$, in DMSO (1×10^{-5} M); the insets are the contours of the molecular orbitals involved in the first vertical excitations. (b) Changes in the light absorbance due to the thermally driven Z-to-E isomerization of the AB-1 and AB-1@BP composites in the DMSO solution at 293 K in the experiment. (c) BP substrate could lower the activation energy, E_a, of the Z-to-E isomerization process and increase ΔE_{Z-E} between the two isomers; the insets are AB-1(Z-down)@BP and corresponding transition-state AB-1(TS)@BP. (d) Energy difference (ΔE_{Z-E}) and binding energy (E_b)/per atom of AB and substituted AB with and without the presence of BP. (e) Calculated (inverted triangle) and experimental (column) values of the Z-to-E activation energy (E_a) of the AB derivatives with and without BP. The charge transfer, δ_{CT}, between AB and BP is also presented. (f) Snapshots of the Z-to-E isomerization of AB-1 on the BP bilayer model with the time evolution of the C−N═N−C torsion angle (ϕ) and the interlayer distance, d, between two adjacent phosphorenes.

substrate are shown in the Supporting Information (Figure S13 and Table S1). Generally, the temperature has no effect on the spectroscopic behavior of azobenzene derivatives, but it strongly enhances the isomerization rate. The thermal isomerization of all four AB derivatives was accelerated by increasing temperature or in the presence of phosphorene. In particular, the rate constant of AB-1@BP (R = $NMe_3^+I^-$) increases by about 23 times compared with that of the free-standing AB-1 at 293 K. The obtained E_a values of the Z-to-E conversion of all AB derivatives and AB@BP hybrids also show the highest reduction of *the* Z-to-E activation energy (0.7 eV) for AB-1 (R = $NMe_3^+I^-$).

As we all know that the freshly prepared phosphorene was not stable under ambient conditions, we also compared the stability of the newly prepared phosphorene with and without AB derivatives. The phosphorene surface adsorbed with AB derivatives lead to significant enhancement (ca. 2.8 times) of the ambient stability compared with free BP (Figure S14).

3.4. Substrate Effect on the Z-to-E Isomerization Rate and Energy Difference Revealed by DFT and RMD Calculations. To gain further insight, DFT calculations with van der Waals correction (vdW-DF2 functional)[39,40] were performed for the AB@BP monolayer and bilayer models. The optimized geometries for different AB derivatives (AB-1−AB-4) are shown in Figure S15. We consider two situations for the Z isomer on phosphorene, with the long alkyl chain lying on the phosphorene surface (called Z-down) and with the unsubstituted benzene ring lying on phosphorene, while the substituted long alkyl chain tilted up (Z-up). E-AB@BP was 0.6−3.0 eV more stable than Z-AB@BP. Z-AB@BP (down) is more stable than Z-AB@BP (up) due to the much larger contact surface. Consequently, the molecule is more energetically favorable to Z-down than Z-up on the phosphorene surface after UV irradiation. The value of the adsorption height, h, was in the range of 3−4 Å, which revealed the physisorption between AB and BP. The absorption height of AB on BP is similar to those predicted for AB adsorbed on other 2D materials, such as arsenene and graphene.[14,41] All of the physisorptions of AB derivatives on BP was energetically favorable with sufficient binding energies, E_b. The negative E_b suggested that both Z/E isomers could stably attached onto phosphorene. In addition, the Z isomer had a shorter absorption height, (h = 3.3 Å) than that (3.5 Å) of the E isomer, implying the stronger interactions between Z-AB and the BP substrate than that in the E-AB. We use the LST−QST method to locate the transition-state structure and to evaluate the Z-to-E isomerization activation energy (E_a) between the *trans* (E) isomer and the *cis* (Z)-(down) isomer on the AB@BP monolayer. The located transition state has a C−N═N−C dihedral at around 90°, suggesting an energetically favorable rotation mechanism. For the studied AB derivatives, the difference in absorption geometry between the Z isomer and the corresponding TS geometry is depicted in Figure S16. The absorption height, h, is defined as the distance between the nitrogen connected to the unsubstituted benzene ring and the upmost atom of the BP surface. As shown in Figure 3c, the adsorption height, h, of AB derivatives (3.3 Å) in the TS structure is much shorter than that (4.1 Å) in the Z-down geometry, indicating that the lone pair in the N═N double bond will interact more strongly with the lone pair of the BP surface. The stronger interaction between the TS geometry and the BP substrate will decrease the energy difference between AB(Z)@BP and AB(TS)@BP, which is the activation energy (E_a) of the Z-to-E isomerization. Hence, the strong interactions between the AB derivatives and the BP substrate could stabilize the Z isomer and transition-state structure less than the E isomer, which decreased the energy barrier of the Z-to-E thermal isomerization and enhanced the energy difference between the Z and E isomers. DFT calculations also predicted that the phosphorene−AB−phosphorene sandwich structure shows a significant increase of energy difference (ΔE_{Z-E}) between the Z/E isomers, ranging from 2.14 to 3.03 eV, which increased by 2−3 times compared with free-standing AB (Figure 3d). Because the AB derivatives differ from each other in the length that contacts the BP substrate, the calculated E_b

https://dx.doi.org/10.1021/acs.jpcc.0c03837
J. Phys. Chem. C 2020, 124, 15961−15968

was divided by the number of atoms, n, of the different AB derivatives to allow a direct comparison of the binding strength between different AB derivatives (Figure 3d).

The electron density difference maps for interactions of AB derivatives and the BP substrate are also shown in Figure S15. In these plots, the isosurface in yellow (cyan) indicates the region of electron gain (loss) due to the interaction. In the AB@BP model, as expected, the long alkyl chain causes charge transfer with the BP substrate. Because nitrogen atoms (both in N═N double bond and in the terminal group, R = NH_2) have higher electronegativity than phosphorus, they pull electrons toward the BP surface, As seen in Figure S15, the presence of the cyan region (electron loss) around the BP surface and a yellow region (electron gain) around the N atom indicated that electrons migrate from BP toward the AB derivatives. Although the bridge oxygen atom (connecting azobenzene and alkyl chain) has a higher electronegativity than phosphorus, we can see the electrons migrate from oxygen (covered by the cyan region) to phosphorus (covered by the yellow region). The highly polar quaternary ammonium salt group (AB-1, R = $NMe_3^+I^-$) induced a much stronger electrostatic interaction with the BP substrate than the others, as reflected by the highest value of E_b/n in AB-1@BP. Bader charge analysis was employed to give a qualitative description of the charge transfer between AB derivatives and the BP substrate. The charge transfer between AB-1, R = $NMe_3^+I^-$ and the BP substrate was approximately 0.1e, which was 10 times larger than for the other AB derivatives (Table S2). There was a correlation between the interfacial charge transfer (CT) and E_a of the AB@BP hybrids. The trend in the calculated activation barriers (inverted triangle) was consistent with the experimental observations (column). For AB without the presence of BP, the terminal groups had a negligible effect on E_a and the free-standing AB derivatives had similar activation energies of about 1.0 eV, but the different binding strengths between the differently substituted ABs and BP caused evident changes of activation barriers in AB@BP with substitutions. Both the predicted and experimental activation energies (E_a) for the Z-to-E isomerization of AB derivatives showed a reduction in E_a in the AB@BP hybrids (Figure 3e).

The RMD simulation scheme, which was developed by our group (with details given in the Supporting Information), was also employed to obtain microscopic pictures of the Z-to-E isomerization process of AB derivatives with and without the BP substrate, respectively. The Z-to-E isomerization process of the AB@BP hybrids finished in a shorter time and more completely than the free-standing AB derivatives.

The Z-to-E isomerization process of AB-**1**@BP hybrids finished in a shorter time (t = 0.6 ps) and more completely (ϕ = 177°) than those of the other species (t = 2.0 ps, ϕ = 150°) (Figure S17). The snapshots showed that four kinds of AB derivatives were flexible with significant changes in the geometry during the Z-to-E isomerization (Figure S18). The tail of molecule AB-**1** seemed to stick on the phosphorene surface due to the strong electrostatic interaction. The Z-to-E isomerization process also increased the interlayer distance of BP to 10 Å (Figure 3f). The RMD simulation also reveals the flexibility of the AB derivatives compared with the DFT calculation.

4. CONCLUSIONS

We used four types of azobenzene derivatives for the noncovalent functionalization of BP nanosheets. As a result, the ambient stability of the newly exfoliated BP nanosheets was enhanced. Moreover, the complexation of AB derivatives with the BP nanosheet could accelerate the Z-to-E isomerization of azobenzene at room temperature. DFT calculations reveal that the strong interactions between AB derivatives and the BP substrate could stabilize the Z isomer and transition-state structure less than the E isomer, which decreased the energy barrier of Z-to-E thermal isomerization and increased the energy difference between Z and E isomers. A close correlation is shown between the extent of charge transfer, binding energy, and the Z-to-E thermal activation energy. Especially, AB with R = $NMe_3^+I^-$ terminal group showed the largest decrease in E_a, probably due to the largest extent of charge transfer with the BP substrate. The predicted energy difference (ΔE_{Z-E}) for the BP−AB−BP sandwich structure was 2−3 times higher than that for free-standing AB. The microscopic picture of the interaction between photoresponsive units and biocompatible 2D nanosheets is useful for the future room-temperature biomedical and energy conversion applications.

■ ASSOCIATED CONTENT

Supporting Information

The Supporting Information is available free of charge at https://pubs.acs.org/doi/10.1021/acs.jpcc.0c03837.

DFT calculations for four kinds of AB derivatives with and without the BP substrate, RMD simulations, and the experimental section (details of fabricating the AB@BP hybrids and characterization) (PDF)

■ AUTHOR INFORMATION

Corresponding Author

Jing Ma − *Key Laboratory of Mesoscopic Chemistry of MOE, School of Chemistry and Chemical Engineering and Jiangsu Key Laboratory of Advanced Organic Materials, School of Chemistry and Chemical Engineering, Nanjing University, Nanjing 210023, Jiangsu, China;* orcid.org/0000-0001-5848-9775; Email: majing@nju.edu.cn

Authors

Dong Zheng − *Key Laboratory of Mesoscopic Chemistry of MOE, School of Chemistry and Chemical Engineering and Jiangsu Key Laboratory of Advanced Organic Materials, School of Chemistry and Chemical Engineering, Nanjing University, Nanjing 210023, Jiangsu, China*

Mengning Ding − *Key Laboratory of Mesoscopic Chemistry of MOE, School of Chemistry and Chemical Engineering, Nanjing University, Nanjing 210023, Jiangsu, China;* orcid.org/0000-0001-6581-3385

Yi Hu − *Key Laboratory of Mesoscopic Chemistry of MOE, School of Chemistry and Chemical Engineering, Nanjing University, Nanjing 210023, Jiangsu, China*

Jun Zhao − *Key Laboratory of Mesoscopic Chemistry of MOE, School of Chemistry and Chemical Engineering, Nanjing University, Nanjing 210023, Jiangsu, China;* orcid.org/0000-0001-7118-4992

Chunyan Liu − *Key Laboratory of Mesoscopic Chemistry of MOE, School of Chemistry and Chemical Engineering, Nanjing University, Nanjing 210023, Jiangsu, China*

Xiang Li − *Key Laboratory of Mesoscopic Chemistry of MOE, School of Chemistry and Chemical Engineering, Nanjing University, Nanjing 210023, Jiangsu, China*

https://dx.doi.org/10.1021/acs.jpcc.0c03837
J. Phys. Chem. C 2020, 124, 15961−15968

Pingying Liu − *Key Laboratory of Mesoscopic Chemistry of MOE, School of Chemistry and Chemical Engineering, Nanjing University, Nanjing 210023, Jiangsu, China*

Zhong Jin − *Key Laboratory of Mesoscopic Chemistry of MOE, School of Chemistry and Chemical Engineering, Nanjing University, Nanjing 210023, Jiangsu, China;* orcid.org/0000-0001-8860-8579

Complete contact information is available at: https://pubs.acs.org/10.1021/acs.jpcc.0c03837

Notes

The authors declare no competing financial interest.

■ ACKNOWLEDGMENTS

This work was supported by the National Key Research and Development Program of China (No. 2019YFC0408303) and the National Natural Science Foundation of China (Nos. 21873045 and 21673111). M.D. acknowledges the support by the Fundamental Research Funds for the Central Universities in China (No. 020514380224) and the Natural Science Foundation of Jiangsu Province (No. BK20180321). Z.J. acknowledges the support by the National Key Research and Development Program of China (Nos. 2017YFA0208200 and 2016YFB0700600), the Fundamental Research Funds for the Central Universities (No. 0205-14380219), the National Natural Science Foundation of China (Nos. 21872069, 51761135104, and 21573108), the Natural Science Foundation of Jiangsu Province (No. BK20180008), and the High-Level Innovation and Entrepreneurship Project of Jiangsu Province of China. The authors are grateful to the High Performance Computing Centre of Nanjing University for providing the IBM Blade cluster system and the support from Nanxin Pharm Co., Ltd., Nanjing.

■ REFERENCES

(1) Li, M.; Luo, Z.; Zhao, Y. Recent Advancements in 2D Nanomaterials for Cancer Therapy. *Sci. China Chem.* **2018**, *61*, 1214−1226.

(2) Xue, Y.; Zhang, Q.; Wang, W.; Cao, H.; Yang, Q.; Fu, L. Opening Two-Dimensional Materials for Energy Conversion and Storage: A Concept. *Adv. Energy Mater.* **2017**, *7*, No. 1602684.

(3) Liu, J.; Cao, H.; Jiang, B.; Xue, Y.; Fu, L. Newborn 2D Materials for Flexible Energy Conversion and Storage. *Sci. China Mater.* **2016**, *59*, 459−474.

(4) Fiori, G.; Bonaccorso, F.; Iannaccone, G.; Palacios, T.; Neumaier, D.; Seabaugh, A.; Banerjee, S. K.; Colombo, L. Electronics Based on Two-Dimensional Materials. *Nat. Nanotechnol.* **2014**, *9*, 768.

(5) Yasaei, P.; Kumar, B.; Foroozan, T.; Wang, C.; Asadi, M.; Tuschel, D.; Indacochea, J. E.; Klie, R. F.; Salehi-Khojin, A. High-Quality Black Phosphorus Atomic Layers by Liquid-Phase Exfoliation. *Adv. Mater.* **2015**, *27*, 1887−1892.

(6) Qiu, M.; Ren, W. X.; Jeong, T.; Won, M.; Park, G. Y.; Sang, D. K.; Liu, L. P.; Zhang, H.; Kim, J. S. Omnipotent Phosphorene: A Next-Generation, Two-Dimensional Nanoplatform for Multidisciplinary Biomedical Applications. *Chem. Soc. Rev.* **2018**, *47*, 5588−5601.

(7) Hüll, K.; Morstein, J.; Trauner, D. In Vivo Photopharmacology. *Chem. Rev.* **2018**, *118*, 10710−10747.

(8) Jia, S.; Fong, W.-K.; Graham, B.; Boyd, B. J. Photoswitchable Molecules in Long-Wavelength Light-Responsive Drug Delivery: From Molecular Design to Applications. *Chem. Mater.* **2018**, *30*, 2873−2887.

(9) Beharry, A. A.; Woolley, G. A. Azobenzene Photoswitches for Biomolecules. *Chem. Soc. Rev.* **2011**, *40*, 4422−4437.

(10) Kolpak, A. M.; Grossman, J. C. Azobenzene-Functionalized Carbon Nanotubes as High-Energy Density Solar Thermal Fuels. *Nano Lett.* **2011**, *11*, 3156−3162.

(11) Feng, W.; Li, S.; Li, M.; Qin, C.; Feng, Y. An Energy-Dense and Thermal-Stable Bis-Azobenzene/Hybrid Templated Assembly for Solar Thermal Fuel. *J. Mater. Chem. A* **2016**, *4*, 8020−8028.

(12) Luo, W.; Feng, Y.; Cao, C.; Li, M.; Liu, E.; Li, S.; Qin, C.; Hu, W.; Feng, W. A High Energy Density Azobenzene/Graphene Hybrid: A Nano-Templated Platform for Solar Thermal Storage. *J. Mater. Chem. A* **2015**, *3*, 11787−11795.

(13) Kucharski, T. J.; Ferralis, N.; Kolpak, A. M.; Zheng, J. O.; Nocera, D. G.; Grossman, J. C. Templated Assembly of Photoswitches Significantly Increases the Energy-Storage Capacity of Solar Thermal Fuels. *Nat. Chem.* **2014**, *6*, 441−447.

(14) Zhao, J.; Liu, C.; Guo, W.; Ma, J. Prediction on the Light-Assisted Exfoliation of Multilayered Arsenene by the Photo-Isomerization of Azobenzene. *Nanoscale* **2017**, *9*, 7006−7011.

(15) Wang, S.; Yue, L.; Li, Z. Y.; Zhang, J.; Tian, H.; Willner, I. Light-Induced Reversible Reconfiguration of DNA-Based Constitutional Dynamic Networks: Application to Switchable Catalysis. *Angew. Chem., Int. Ed.* **2018**, *57*, 8105−8109.

(16) Frisch, M.; Trucks, G.; Schlegel, H.; Scuseria, G.; Robb, M.; Cheeseman, J.; Scalmani, G.; Barone, V.; Mennucci, B.; Petersson, G. *Gaussian 09*, revision D.01; Gaussian Inc.: Wallingford, CT, 2009.

(17) Enkovaara, J.; Rostgaard, C.; Mortensen, J. J.; Chen, J.; Dułak, M.; Ferrighi, L.; Gavnholt, J.; Glinsvad, C.; Haikola, V.; Hansen, H.; et al. Electronic Structure Calculations with GPAW: A Real-Space Implementation of the Projector Augmented-Wave Method. *J. Phys.: Condens. Matter* **2010**, *22*, No. 253202.

(18) Kresse, G.; Joubert, D. From Ultrasoft Pseudopotentials to the Projector Augmented-Wave Method. *Phys. Rev. B* **1999**, *59*, No. 1758.

(19) Perdew, J. P.; Burke, K.; Ernzerhof, M. Generalized Gradient Approximation Made Simple. *Phys. Rev. Lett.* **1996**, *77*, No. 3865.

(20) Monkhorst, H. J.; Pack, J. D. Special Points for Brillouin-Zone Integrations. *Phys. Rev. B* **1976**, *13*, No. 5188.

(21) Halgren, T. A.; Lipscomb, W. N. The Synchronous-Transit Method for Determining Reaction Pathways and Locating Molecular Transition States. *Chem. Phys. Lett.* **1977**, *49*, 225−232.

(22) *Materials Studio*, version 4.0; Accelrys Inc.: San Diego, 2006.

(23) Momma, K.; Izumi, F. Vesta 3 for Three-Dimensional Visualization of Crystal, Volumetric and Morphology Data. *J. Appl. Crystallogr.* **2011**, *44*, 1272−1276.

(24) Tian, Z.; Wen, J.; Ma, J. Dynamic Simulations of Stimuli-Responsive Switching of Azobenzene Derivatives in Self-Assembled Monolayers: Reactive Rotation Potential and Switching Functions. *Mol. Simul.* **2015**, *41*, 28−42.

(25) Wen, J.; Tian, Z.; Ma, J. Light-and Electric-Field-Induced Switching of Thiolated Azobenzene Self-Assembled Monolayer. *J. Phys. Chem. C* **2013**, *117*, 19934−19944.

(26) Liu, P.; Liu, C.; Liu, Q.; Ma, J. Influence of Photoisomerization on Binding Energy and Conformation of Azobenzene-Containing Host-Guest Complex. *Acta Phys.-Chim. Sin.* **2018**, *34*, 1171−1178.

(27) Tian, Z.; Wen, J.; Ma, J. Reactive Molecular Dynamics Simulations of Switching Processes of Azobenzene-Based Monolayer on Surface. *J. Chem. Phys.* **2013**, *139*, No. 014706.

(28) Liu, C.; Zheng, D.; Hu, W.; Zhu, Q.; Tian, Z.; Zhao, J.; Zhu, Y.; Ma, J. Tuning the Collective Switching Behavior of Azobenzene/Au Hybrid Materials: Flexible Versus Rigid Azobenzene Backbones and Au(111) Surfaces Versus Curved Au Nanoparticles. *Nanoscale* **2017**, *9*, 16700−16710.

(29) Sun, H. Ab Initio Calculations and Force Field Development for Computer Simulation of Polysilanes. *Macromolecules* **1995**, *28*, 701−712.

(30) Ribeiro, H. B.; Pimenta, M. A.; de Matos, C. J. Raman Spectroscopy in Black Phosphorus. *J. Raman Spectrosc.* **2018**, *49*, 76−90.

(31) Luo, W.; Zemlyanov, D. Y.; Milligan, C. A.; Du, Y.; Yang, L.; Wu, Y.; Peide, D. Y. Surface Chemistry of Black Phosphorus under a

Controlled Oxidative Environment. *Nanotechnology* **2016**, *27*, No. 434002.
(32) Wang, C.; et al. Monolayer Atomic Crystal Molecular Superlattices. *Nature* **2018**, *555*, 231−236.
(33) Banghart, M. R.; Volgraf, M.; Trauner, D. Engineering Light-Gated Ion Channels. *Biochemistry* **2006**, *45*, 15129−15141.
(34) Banghart, M.; Borges, K.; Isacoff, E.; Trauner, D.; Kramer, R. H. Light-Activated Ion Channels for Remote Control of Neuronal Firing. *Nat. Neurosci.* **2004**, *7*, 1381.
(35) Yu, G.; Han, C.; Zhang, Z.; Chen, J.; Yan, X.; Zheng, B.; Liu, S.; Huang, F. Pillar[6]Arene-Based Photoresponsive Host-Guest Complexation. *J. Am. Chem. Soc.* **2012**, *134*, 8711−8717.
(36) Döbbelin, M.; et al. Light-Enhanced Liquid-Phase Exfoliation and Current Photoswitching in Graphene−Azobenzene Composites. *Nat. Commun.* **2016**, *7*, No. 11090.
(37) Feng, Y.; Liu, H.; Luo, W.; Liu, E.; Zhao, N.; Yoshino, K.; Feng, W. Covalent Functionalization of Graphene by Azobenzene with Molecular Hydrogen Bonds for Long-Term Solar Thermal Storage. *Sci. Rep.* **2013**, *3*, No. 3260.
(38) Garcia-Amorós, J.; Díaz-Lobo, M.; Nonell, S.; Velasco, D. Fastest Thermal Isomerization of an Azobenzene for Nanosecond Photoswitching Applications under Physiological Conditions. *Angew. Chem.* **2012**, *124*, 12992−12995.
(39) Klimeš, J.; Bowler, D. R.; Michaelides, A. Chemical Accuracy for the Van Der Waals Density Functional. *J. Phys.: Condens. Matter* **2009**, *22*, No. 022201.
(40) Klimeš, J.; Bowler, D. R.; Michaelides, A. Van Der Waals Density Functionals Applied to Solids. *Phys. Rev. B* **2011**, *83*, No. 195131.
(41) Zhao, J.; Ma, J. Theoretical Designs of Photoresponsive Energy-Storage Materials Based on Attachment of Π-Conjugated Molecules onto Sulfur-Doped Graphene. *J. Phys. Chem. C* **2016**, *120*, 25131−25141.

https://dx.doi.org/10.1021/acs.jpcc.0c03837
J. Phys. Chem. C 2020, 124, 15961−15968